Journal of Materials Chemistry A

RSC Publishing

PAPER

View Article Online
View Journal

Cite this: DOI: 10.1039/c3ta12303k

Silicon alkoxide cross-linked silica nanoparticle gels for encapsulation of bacterial biocatalysts

Baris R. Mutlu,[a] Sujin Yeom,[b] Ho-Wang Tong,[a] Lawrence P. Wackett[cd] and Alptekin Aksan*[ad]

Received 13th June 2013
Accepted 24th July 2013

DOI: 10.1039/c3ta12303k

www.rsc.org/MaterialsA

A method is developed for encapsulation of bacterial biocatalysts in silica gels formed by silica nanoparticles (SNP) and a silicon alkoxide crosslinker. Formulation of the gel was optimized by changing the SNP size, SNP to crosslinker ratio and crosslinker functionality. Hydrolysis and condensation reactions of silicon alkoxide were controlled by water to alkoxide ratio (*r*) and pH of the solution. FTIR analysis verified that a reactive and temporally stable silicon alkoxide crosslinker was obtained. As a case study, recombinant *Escherichia coli (E. coli)* cells expressing the atrazine dechlorinating enzyme AtzA were encapsulated. Synthesized catalytic biomaterials (silica gel encapsulated bacterial biocatalysts) were evaluated based on their gelation time, biocatalytic activity and mechanical strength. Diffusivity assays and SEM were used for characterization of the gel structure. We found that SNP to crosslinker ratio affected all the features of the gel, whereas crosslinker functionality primarily affected the gelation time and SNP size affected the mechanical strength and diffusivity. Based on systematic evaluation, we selected three gel formulations and subjected them to long-term activity measurements in a continuous-flow bioreactor for removing trace levels of atrazine. The effluent atrazine concentration was sustained below 30% of the influent concentration, <3 ppb, for 2 months.

Introduction

Silica gels have been extensively studied for encapsulation of whole cells for different applications in biotechnology and biomedical engineering.[1–5] In most of these applications, ensuring biocompatibility (*i.e.* encapsulated cell viability) during the encapsulation process and in the resulting gel has been a major challenge. Many studies were conducted to increase the biocompatibility of the encapsulation processes[6] by removing the alcohol produced by the gelation process[7] or by incorporating additives (such as polyethylene glycol (PEG), glycerol) into the gel.[8,9] However, recent studies reported that biocompatibility is not essential for biocatalysis applications where a thermodynamically favorable reaction is catalyzed by intracellular enzymes. For example, Fennouh *et al.* reported catalytic activity in silica gels that contained encapsulated *E. coli* cells with compromised cell membranes (observed by electron microscopy),[10] Nassif and Livage suggested that encapsulated bacteria can function as a "bag of enzymes" even if they had compromised membrane integrity.[11] In two different studies,[12,13] it was shown that activity of the intracellular enzyme β-galactosidase increased significantly when encapsulated *E.coli* were treated with organic solvents to enhance the permeability of the cell membrane (and by potentially compromising it). These results showed that for biocatalysis applications that do not require cell viability, steps to increase biocompatibility (such as alcohol removal during encapsulation or incorporation of costly organic polymer additives to protect the cells) can be eliminated. In the present study, our aim was to sustain and potentially enhance biocatalytic activity while preventing leakage of intracellular enzymes from the biomaterial. Moreover, we sought to keep the cost of the process and the biomaterials low by bypassing the need to preserve cell viability.

Gel microstructure directly affects diffusivity of the chemicals through, and the mechanical strength of the porous silica material. Therefore, it is desirable to develop encapsulation methods that maintain catalytic activity of the encapsulated organisms, while simultaneously optimizing the chemical and physical properties of the gels. The conventional silica gel encapsulation method is the sol–gel transition of a silicon alkoxide.[14] In a typical process, a silicon alkoxide such as tetraethyl orthosilicate (TEOS) is hydrolyzed in the presence of water and an acidic catalyst. Depending on the pH and temperature of the solution, the reactive silanol (Si–OH) groups of the hydrolyzed silicon alkoxide go through condensation reactions to form siloxane (Si–O–Si) bonds, developing a 3D porous gel structure. The cells are added to the solution after

[a]Department of Mechanical Engineering, University of Minnesota, Minneapolis, MN 55455, USA. E-mail: aaksan@umn.edu

[b]Department of Microbiology, University of Minnesota, Minneapolis, MN 55455, USA

[c]Department of Biochemistry, Molecular Biology and Biophysics, University of Minnesota, Minneapolis, MN 55455, USA

[d]BioTechnology Institute, University of Minnesota, Saint Paul, MN 55108, USA

the hydrolysis reaction is completed and they get entrapped within the gel during the condensation process (polymerization). One limitation of this method is realized when the cells are exposed to acid, which can hamper the activity of the intracellular enzymes or inactivate them irreversibly. To eliminate this problem, the common practice is to adjust the pH of the solution before adding cells. While neutralization of the pH can preserve enzyme activity, it may sacrifice gel microstructure control, resulting in gels of inadequate diffusion or inferior mechanical properties.

Silica nanoparticles (SNPs) are also appealing as precursors for silica encapsulation of bacteria due to their commercial availability at high volumes and low cost. SNPs are available in various sizes ranging from nanometers to micrometers, enabling the microstructure of a silica gel to be fine-tuned by using SNPs of different diameters. SNPs are commonly stabilized in highly alkaline solutions and by lowering the pH of the solution it is possible to obtain a gel. Finnie *et al.* have shown that sulfate-reducing bacteria can be encapsulated in such a gel obtained by lowering the pH of Ludox SM-30 SNP sol.[15] However, cell encapsulation by using SNPs exclusively enables limited control on the process and the properties of the formed gel. Therefore, SNPs are more commonly used in combination with other precursors such as sodium silicate.[13] However, it was reported that mechanical stability, as determined by Young's modulus of the gel, of sodium silicate + SNP gels decreases when the SNP concentration is increased.[16] Therefore, in this study, we opted to use a silicon alkoxide precursor (TEOS or MTES) to act as a crosslinker for the SNPs. After the pH of the SNP sol was neutralized, the bacteria were mixed with the aqueous sol and hydrolyzed silicon alkoxide was added to induce cross-linking and foster polymerization. Using this approach, it was possible to fine-tune the microstructure, and therefore the diffusivity of the gel, by altering the SNP size. A range of SNP to silicon alkoxide ratios were investigated to ensure formation of an SNP-governed microstructure and silicon alkoxide functionality was investigated for its potential effects on the process and gel structure.

We applied the methods described above to an important practical problem, using recombinant *E. coli* cells expressing the atrazine dechlorinating enzyme AtzA to transform atrazine to hydroxyatrazine. Atrazine (2-chloro-4-ethylamine-6-isopropylamino-*s*-triazine) is one of the most commonly used agricultural herbicides in the U.S. and its concentration in drinking water is regulated by Environmental Protection Agency (EPA). The World Health Organization (WHO) determined an acceptable daily intake limit of 0.1 mg L^{-1} (~100 ppb) for atrazine in drinking water;[17] whereas EPA determined an upper limit of 3 ppb as an annual average.[18] Currently, atrazine is removed from drinking water by filtration methods that rely on adsorption, most commonly activated carbon, that has to subsequently be disposed of or incinerated for re-charging. In this regard, a biocatalytic material that degrades atrazine is desirable for environmental sustainability provided that it is cost competitive. The overall challenges for a silica-based bioremediation system are that it needs to: (1) function well with trace levels of atrazine found in drinking water (<10 ppb), (2) sustain function for weeks or months in a continuous, flow-through process, (3) be mechanically strong and stable under continuous flow conditions.

Successful applications of atrazine bioremediation at high concentrations (samples from farm run-off waters or buffer solutions fortified with atrazine), from 10 to 30 ppm, have been reported[19–22] but most laboratory studies have used much higher atrazine concentrations that do not mimic actual environmental situations. Galindez-Najera *et al.* reported complete removal (*i.e.* effluent concentration below detection limit of assay) of atrazine using a two-stage biofilm reactor with a binary culture of *Stenotrophomonas maltophilia* and *Arthrobacter* sp., at over 30 000 ppb influent atrazine concentration.[20] Liu *et al.* reported above 90% removal efficiency of atrazine from wastewater using a membrane bioreactor containing *Pseudomonas* sp. ADP, at ~15 000 ppb influent atrazine concentration.[21] While these approaches are suitable for removal of atrazine at high concentrations, effluent concentrations are still significantly higher than 3 ppb, despite the high removal efficiency. In a recent study, Buttigleri *et al.* utilized a membrane bioreactor (MBR) with a denitrifying mixed culture atrazine treatment at low concentrations.[23] With a 10 ppb influent concentration, an average removal of 15% was obtained over a 3 month period. In addition to the low performance of the reactor at low atrazine concentrations, it is also not desirable to have living bacteria in a reactor for drinking water treatment. This requires further downstream processing to ensure that any bacteria that may leach from the system are removed from water, increasing the overall cost of the system.

Our research group recently encapsulated recombinant *E. coli* cells expressing atrazine dechlorinating enzyme AtzA into silica gels and the cells were killed by a post-encapsulation heat treatment process. Batch activity tests were run with an ~30 000 ppb atrazine solution and biocatalytic activity of non-viable encapsulated cells (0.44–0.66 μmol g^{-1} cells per min) was comparable to free cell activity (0.61 μmol g^{-1} min^{-1}) but sustained for a much longer time, 4 months, compared to free cells.[24] However, at low concentrations of atrazine (10 ppb), the biocatalytic activity of the cells was several orders of magnitude lower and the atrazine degradation of the encapsulated cells in a packed bed reactor gradually decreased to an immeasurable rate within 2 weeks. Mechanical integrity of the gels was also shown to degrade significantly during that time (data not shown).

To overcome the limitations of the previous studies, while also developing an economically feasible product, the present study sought to develop catalytic silica biomaterials that maintained high atrazine removal rates for long durations at a low influent concentration. Utilizing three of the developed formulations in a flow-through packed bed reactor system, effluent atrazine concentration was maintained at a level below 30% of the 10 ppb influent for 2 months. Additionally, as compared to our previous study,[24] mechanical strength of the material was improved from a yield load of 0.2 N to a maximum of 3 N and cost of the product is significantly reduced by eliminating high cost silica precursors and organic polymer additives from the formulation. The design was conducted

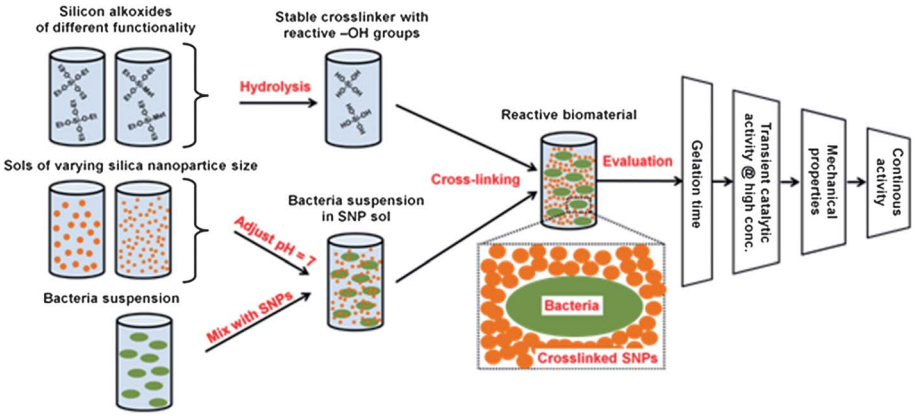

Fig. 1 Schematic of encapsulation and evaluation methods.

through a step-by-step evaluation/elimination process, based on biomaterial characteristics such as gelation time, transient catalytic activity at high concentration and mechanical strength (Fig. 1). Additional characterization studies (diffusivity and cell viability assays, SEM) were also performed for better interpretation of the results. Our results suggest that the developed catalytic biomaterial(s) can be used for continuous treatment of water to remove environmentally-relevant concentrations of atrazine from drinking water. On a broader note, the proposed method can also be used to encapsulate different biocatalysts, aimed to treat other low concentration contaminants (pharmaceuticals, personal care products, endocrine disruptors, *etc.*) from drinking water supplies.

Experimental

Materials

Tetraethoxysilane (TEOS: $Si(OC_2H_5)_4$) and triethoxymethylsilane (MTES: $CH_3Si(OC_2H_5)_3$) of reagent and technical grades, respectively were purchased from Sigma-Aldrich (Sigma-Aldrich Corp. St. Louis, MO, USA). Ludox HS40 and Ludox TM40 SNP sols were purchased from Sigma-Aldrich and NexSil 85-40 and NexSil 125-40 SNP sols were generously provided by Nyacol (Nyacol Nano Technologies Inc., Ashland, MA, USA). All the SNP sols had 40% SiO_2 content by mass and were stabilized by sodium ions. The only difference between different SNPs is the nanoparticle size and their initial pH, as shown in Table 1. Technical grade atrazine was provided by Syngenta (Syngenta Crop Protection, NC, USA). All the chemicals were used as received. Ultrapure water (UPW) was used in all the experiments. UPW was prepared by filtering deionized water through a Milli-Q water purification system (Millipore, Billerica, MA, USA) to a final electrical resistance of >18.2 MΩ cm^{-1}.

Bacterial strains and growth conditions

The growth conditions were identical to those described previously, except for some minor modifications.[24] *E. coli* DH5 α (pMD4)[25] was grown at 37 °C in superbroth medium with vigorous aeration, supplemented with 30 μg mL^{-1} chloramphenicol. Intermediate cultures were grown by inoculation with 1% (v/v) starter culture and diluted 100-fold in production flasks containing the same medium. Cells were harvested by centrifugation at 6000×*g* for 20 min at 4 °C.

Catalytic biomaterial synthesis and encapsulation

Hydrolysis and condensation reactions of silicon alkoxides were controlled by adjusting water to silicon alkoxide molar ratio (*r*) and pH of the solution. 1 : 5.3 : 0.0013 molar ratio of silicon alkoxide : water : HCl was used to obtain $r = 5.3$ and a pH of 4, which resulted in a fully-hydrolyzed silicon alkoxide solution with a slow condensation rate. The values for *r* and pH were selected based on previous literature reports. Brinker reported that, during hydrolysis with sub-stoichiometric amounts of water ($r < 4$), condensation starts before complete hydrolysis and alcohol-producing condensation reactions are favored.[26] However, increasing *r* excessively can promote depolymerization of the gel by siloxane bond cleavage reactions. Therefore, an *r* value that is slightly over 4 was selected. In the pH 3–8 range, hydrolysis rate of alkoxysilanes increases when acidity or alkalinity of the solution increases and condensation rate increases with increased alkalinity.[27] Therefore, the pH of the solution was adjusted to 4 to obtain fast hydrolysis and slow condensation reactions. This ensured that the silicon alkoxide did not polymerize by itself but cross-linked the SNPs. The hydrolyzed silicon alkoxides were kept in an ice bath until they were used to further slow down condensation reactions.

For verification of the desired (fully hydrolyzed, slow condensation) state of the silicon alkoxide, progress of the hydrolysis and condensation reactions were observed by IR spectroscopy. After the initial phase separation of the silicon

Table 1 Properties of the SNP sols used in this study

Commercial name	Abbreviation	Average particle diameter [nm]	Density [g mL^{-1}]	Initial pH
Ludox HS40	HS40	12	1.3	9.7
Ludox TM40	TM40	22	1.3	9.0
Nexsil 85-40	NS85	50	1.2	9.5
Nexsil 125-40	NS125	85	1.2	9.5

alkoxide–water–HCl solution disappeared, 0.15 μL samples were extracted from the solution in 15 minute time intervals. Samples were placed between two BaF_2 windows. The windows were sealed with vacuum grease to prevent evaporation. The sealed sample was transferred to an infrared microscope attached to an FTIR spectrometer (Thermo-Nicolet Continuum equipped with a Mercury Cadmium Telluride detector, Thermo Electron, Waltham, MA, USA). The FTIR sampling resolution was 4 cm^{-1}, and 128 IR scans were averaged per spectrum in the 4000–740 cm^{-1} wavenumber range. The IR spectra were analyzed using OMNIC (Thermo-Nicolet) software. This experiment was run in duplicate. The state of hydrolysis and condensation reaction rates was determined by measuring the intensity of δ-OH bending peak of water at 1650 cm^{-1} and the CH_3 bending peak of silicon alkoxide (TEOS, MTES) and produced ethanol at 1384 cm^{-1}.

The pH of the SNP sol was adjusted to neutral pH by adding 1 M hydrochloric acid to avoid inactivation of the enzyme and to eliminate initial pH variations between different SNP sols. After pH adjustment, bacteria were momentarily suspended in a 1 g mL^{-1} aqueous suspension and added to the SNP sol. The added amount was adjusted such that the final concentration of encapsulated bacteria in the gel was 0.125 grams mL^{-1} of silica precursor (SNPs and silicon alkoxide combined).

Silicon alkoxide was added to the bacteria + SNP solution by pipetting a few times to obtain a homogeneous sample. SNP sol to silicon alkoxide ratios were selected as 7 : 1, 3 : 1 and 1 : 1 (v/v). Mass contribution of silica precursors to the gel microstructure can be estimated using two assumptions: (1) silicon alkoxide is fully hydrolyzed (2) all SNPs are cross-linked by silicon alkoxide. With these assumptions, Table 2 shows the estimated silica content contribution from different precursors of the gels.

The final product was either placed in molds or vials for gelation, depending upon the specifics of the experiment to be conducted. The gelation occurred within seconds to hours depending on the formula used. For molding of fast gelation time formulations, precursors were cooled by immersion in an ice bath to slow gelation. During gelation and storage, the vials were kept closed and molds were sealed with a PVDC film to prevent drying.

Characterization

Gelation time. Biomaterials were synthesized in glass scintillation vials and gently shaken intermittently to determine the degree of crosslinking of the gel. The time intervals between observations were increased with increasing duration of the experiment. Gelation time was determined as the time when solution in the container no longer exhibited observable flow when agitated.

Biocatalytic activity assays. Catalytic activity of the biomaterial is determined by transient and steady-flow activity assays. In transient activity assays, biomaterials were synthesized in glass scintillation vials as 2 mL cylindrical blocks (3.5 mm thickness and ~570 mm^2 surface area), in triplicate. Three mL of 150 μM (32.4 ppm) atrazine solution in 0.1 M potassium phosphate buffer (at pH 7.0) was added on top of each gel and vials were placed on a rotary shaker. Samples were collected after 60 min of incubation and immediately immersed in a 90 °C water bath to stop their catalytic activity by denaturing the enzyme. After inactivation of the enzyme, samples were filtered through a 0.2 μm pore size PTFE syringe filter to remove any particulates that may be released from the material. The concentrations of atrazine and its metabolite, hydroxyatrazine, were measured by using high performance liquid chromatography (HPLC) as described by de Souza *et al.*[25] Transient activity assays were performed right after encapsulation (day 0) and after 4 days of storage within scintillation vials at room temperature. The vials were kept tightly closed to prevent samples from drying.

For steady-flow activity measurements, biomaterials were synthesized in stainless steel molds as hemispherical beads of 1.5 mm diameter. 6.6 grams of beads were transferred into 15 mL glass bioreactors (Buchner funnels, coarse grade) that were connected to a peristaltic pump drive (Masterflex L/S variable speed modular drive, Cole-Parmer, Vernon Hills, IL, USA). Ten ppb atrazine solution in 0.1 M potassium phosphate buffer (at pH 7.0) was used as influent solution to the bioreactors and was replenished whenever required during experimentation. A slow flow rate of 0.05 mL min^{-1} was chosen to maximize residence time (5 hours) and minimize the produced effluent water. Collected samples were treated as previously described and concentration of atrazine in the effluent fluid was measured using the Atrazine Plate Kit (Beacon Analytical Systems Inc., USA) in accordance with the manufacturer's instructions.

Mechanical properties. Mechanical tests were performed on hemispherical beads (in triplicate) which were synthesized as previously described. A uniaxial testing machine was used with a 5 N load cell with 0.05 N resolution (Instron, Norwood, MA, USA). During testing, constant displacement rate was applied to the material until the material failed. Results were obtained in the form of a load-displacement curve.

Cell viability assay. Catalytic biomaterials were synthesized in scintillation vials. A 0.1 g aliquot of the material was pulverized using a mortar and pestle and the crushed material was suspended in 2 mL of sterile phosphate-buffered saline. The solution was serially diluted and spread-plated onto Luria–Bertani agar with 10 μg mL^{-1} chloramphenicol in triplicate. Cell counts were determined based on the number of observed Colony Forming Units (CFUs) after overnight incubation.

Table 2 Total silica contribution ratio of SNP sol/crosslinker by mass based on volumetric ratio

Crosslinker	TEOS			MTES	
SNP sol/crosslinker (v/v)	7 : 1	3 : 1	1 : 1	7 : 1	3 : 1
Ludox HS40	8.45	3.62	1.20	7.54	3.23
Ludox TM40	8.45	3.62	1.20	7.54	3.23
Nexsil 85-40	7.80	3.34	1.11	6.96	2.98
Nexsil 125-40	7.80	3.34	1.11	6.96	2.98

Diffusivity assay. Trypan blue solution (0.4%) purchased from Sigma (Sigma-Aldrich Corp. St. Louis, MO, USA) was used to evaluate the diffusivity of the synthesized gels. Four hundred μL of gels without cells were synthesized in polystyrene cuvettes with 10 × 4 mm base dimensions. One hundred μL of Trypan blue solution was added on top of the gel and progress of the dye diffusion in the gel was recorded by taking a picture every hour for 6 hours.

The diffusivity of the dye in the gel was evaluated by using the error function solution of the 1D diffusion problem with constant concentration boundary condition:[28]

$$C(x,t) = C_{BC} \times \mathrm{erfc}\left(\frac{x}{2\sqrt{Dt}}\right)$$

In this equation C is concentration, x is distance from the boundary, C_{BC} is fixed boundary condition concentration, t is time and D is diffusivity. To solve for D, we have used a 4 step image processing technique: (1) the images were converted to grayscale, (2) the intensity values of the pixels were averaged along the horizontal axis, (3) $C(x)/C_{BC}$ was determined from the ratio of the averaged intensity along a given horizontal axis at distance x over the averaged intensity at x_0 – averaged intensity at x_∞ (far enough from the boundary such that boundary condition has no effect), (4) x values corresponding to $C(x)/C_{BC} = 0.1$, 0.2 and 0.3 were determined and obtained D values were averaged. All the image processing and computations were done using MATLAB.

Microstructure. Gel and encapsulated bacteria were examined by scanning electron microscopy (Hitachi S-4700). The encapsulated bacteria were fixed in 2% glutaraldehyde and then 1% osmium tetroxide in cacodylate buffer (0.1 M sodium cacodylate, pH 7.3). After fixation, the samples were gradually dehydrated in an up-grading series of ethanol (50, 70, 80, 95 and 100%). The samples were then dried in a Critical Point Dryer (Tousimis Model 780A) using liquid carbon dioxide as transitional fluid. Finally, the samples were sputter-coated with a thin layer of gold–palladium and examined under the SEM.

Results and discussion

In reporting the results, different gel formulations are denoted as SNP – SNP to crosslinker ratio (v/v) – Crosslinker type (example: HS40-3 : 1-TEOS).

State of hydrolysis and condensation reactions of silicon alkoxide crosslinkers

After 1 hour of stirring, it was visually observed that the mixture became miscible in both TEOS and MTES solutions. This is due to destruction of water and production of ethanol during hydrolysis reactions. Based on the TEOS–water–ethanol ternary phase diagram, it is expected that ~85% of the water was hydrolyzed at this point.[29] Fig. 2 shows the collected IR spectra from samples in terms of normalized ratio of δ-OH bending peak of water to CH_3 bending peak (actual spectra shown on inset) between 1 and 3 hours at 15 minute intervals. In both TEOS and MTES solutions, the ratio initially decreased for 15 to 30 minutes, indicating continuing hydrolysis. Then the water content in the solution started increasing with respect to the total amount of CH_3, contributed from both silicon alkoxide and produced ethanol during hydrolysis reactions. This shows that hydrolysis was completed and condensation reactions were taking place, as expected based on the selected r and pH of the solution. It can also be seen that the ratio increased very slowly, indicating that condensation rate was low and the hydrolyzed silicon alkoxide solution was stable over time. It should be noted that while samples were being transferred to the BaF_2 windows, it is possible that minute volumes of ethanol have evaporated. This would increase the H_2O to CH_3 amplitude ratio and explain the variation in the data points. Hence, it is possible that the increase is due to a combined effect of condensation reactions and ethanol evaporation, which means that silicon alkoxide solution is more stable than suggested by the data. Since we only seek to show temporal stability over the duration of encapsulation process, we have stopped FTIR analysis after 3 hours. Stability of the silicon alkoxide solution is also verified by leaving the hydrolyzed silicon alkoxide solution (both TEOS and MTES) in a scintillation vial without addition of SNPs. No gelation was observed within 2 days of storage at room temperature.

Silica gel: gelation time, diffusivity, mechanical properties and microstructure

Materials were initially characterized by their time to gel, as shown in Table 3. Gels cross-linked by MTES gelled in the time-scale of hours, whereas gels with TEOS crosslinker gelled within seconds to minutes. It was also observed that increasing SNP size and SNP to crosslinker ratio increased gelation time. In fast gelation time formulations, insertion in an ice bath was sufficient to slow down crosslinking for molding. In the range of our experiments, the most prominent factor that affected gelation time was the functionality of the silicon alkoxide crosslinker.

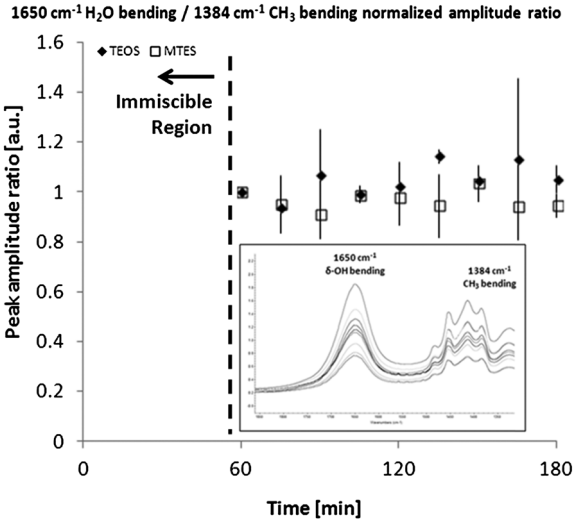

Fig. 2 Evaluation of the hydrolysis/condensation process by evolution of the peak amplitude ratio of δ-OH bending/CH_3 bending.

This result can be attributed to trifunctional MTES having less reactive sites for siloxane bond formation compared to tetrafunctional TEOS. This result is in accordance with the observations of Innocenzi *et al.*,[30] who observed an increase in gelation time of TEOS/MTES gels with increasing MTES content. Another result was that gelation time increased when SNP to crosslinker ratio increased and larger SNPs were used. This can be explained by the decrease in the total number of reactive sites per volume, as SNP content increases or nanoparticles get larger.

Effective diffusivity of the Trypan blue dye in the selected gels is shown in Fig. 3. It can be observed that the highest diffusivities were around 2.25×10^{-4} mm^2 s^{-1} and were obtained with largest size (NS125 ~85 nm) nanoparticles. In all gels, diffusivity decreased with decreasing SNP size, except for HS40-3 : 1-MTES gel. Data from the 1 : 1-TEOS gels and HS40-3 : 1-TEOS gel are not shown due to observed rapid propagation of the dye through cracks within the gel due to gravitational force instead of diffusion. Dye diffusivity experiments show that the diffusivity of the gel can be controlled by varying the SNP size. It was also observed that the effect of SNP size on diffusivity is the most significant in 7 : 1-TEOS gels and least significant in 3 : 1-TEOS gels. This can be explained by SNP size having more effect on the microstructure in 7 : 1 SNP to crosslinker ratio gels as compared to 3 : 1 gels. This can also be observed in Fig. 4. In 12 nm SNPs (HS40), when SNP to crosslinker ratio was 7 : 1, SNPs were linked to each other with no observable crosslinker. However, when the ratio decreased to 1 : 1 (*i.e.* crosslinker content increased), SNPs were linked together with observable crosslinker. Note that the particles in 1 : 1 ratio appear slightly larger, because of crosslinker deposition on the surface before crosslinking. Similar effect of SNP to crosslinker ratio was observed for 50 nm SNPs (NS85). In 7 : 1 SNP to crosslinker ratio, particles were linked together with small area of contact. In 1 : 1 ratio, smaller aggregates of silica were observed along with the SNPs, formed by condensation reactions of the crosslinker. Note that even though the silicon alkoxide is stable in low pH conditions of the hydrolysis, when SNPs are introduced the pH of the solution rises and condensation reactions are unavoidable. Perullini *et al.* reported the effect of SNP content on diffusivity in sodium silicate + SNP gels, where diffusivity of cationic dye Crystal Violet was used as a model. They reported that transport was faster when the gel was richer in SNPs.[16] We observed a similar trend only in TEOS cross-linked NS125-7 : 1 and NS85-7 : 1 gels. For MTES cross-linked gels, the effect of SNP to crosslinker ratio did not have a significant effect on gel diffusivity. The decreasing effect of larger SNP size on gel diffusivity was observed in all MTES gels, except for TM40 to HS40 transition in 3 : 1 gels. Encapsulated cells in silica gel are shown in Fig. 5.

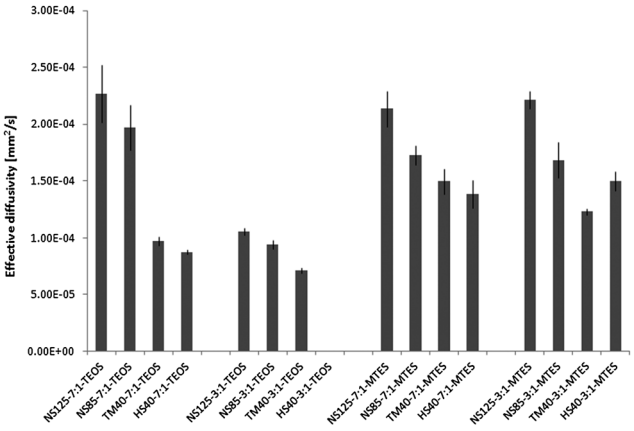

Fig. 3 Effective diffusivity of the selected gels.

It should be noted that, a macroporous structure was observed in SEM micrographs of the NS85-3 : 1-TEOS gel. This was caused by excessive crosslinker deposition on the SNP surface and large SNP size. However, it is interesting that this macroporous structure was not conserved when SNP to crosslinker ratio was increased to 7 : 1 or SNP size was increased to ~85 nm (NS125 SNPs). One would expect to see increased diffusion rates of NS85-3 : 1-TEOS gel, with increased porosity seen in SEM images, however this was not the case as shown in Fig. 3. Therefore, microstructures of the gels (especially the conditions leading to the observed macroporous structure of NS85-3 : 1-TEOS gel) needs to be further investigated in future studies.

Mechanical properties of different samples were evaluated on the basis of load at compressive yield (Fig. 6). In both TEOS and MTES cross-linked gels, best mechanical properties were obtained with the smallest size SNPs (HS40 and TM40 respectively) and there was a decreasing trend in load at compressive yield when SNP size was increased. When 12 nm size HS40 SNPs were used, decreasing the SNP to crosslinker ratio decreased the load at compressive yield of the gel. On the contrary, when 85 nm size NS125 SNPs were used, the effect was reversed. Independent from the crosslinker functionality, we observed a

Table 3 Gelation times for the catalytic biomaterials synthesized with selected parameters (gelation times are given as: seconds (s): t_{gel} < 1 min, minutes (min): 1 min < t_{gel} < 10 min, hour (h): 10 min < t_{gel} < 2 hours and hours (hrs): t_{gel} > 2 hours)

SNP sol	Ludox HS40			Ludox TM40			Nexsil 85-40		Nexsil 125-40		
Crosslinker	TEOS		MTES	TEOS		MTES	TEOS	MTES	TEOS	MTES	
SNP to crosslinker ratio (v/v)	3 : 1	7 : 1	7 : 1	3 : 1	7 : 1	7 : 1	7 : 1	7 : 1	7 : 1	3 : 1	7 : 1
	1 : 1		3 : 1	1 : 1		3 : 1	3 : 1	3 : 1	3 : 1	1 : 1	
			1 : 1			1 : 1	1 : 1	1 : 1	1 : 1		
Approximate gelation time	s	min	h	s	min	h	min	h	min	h	hrs

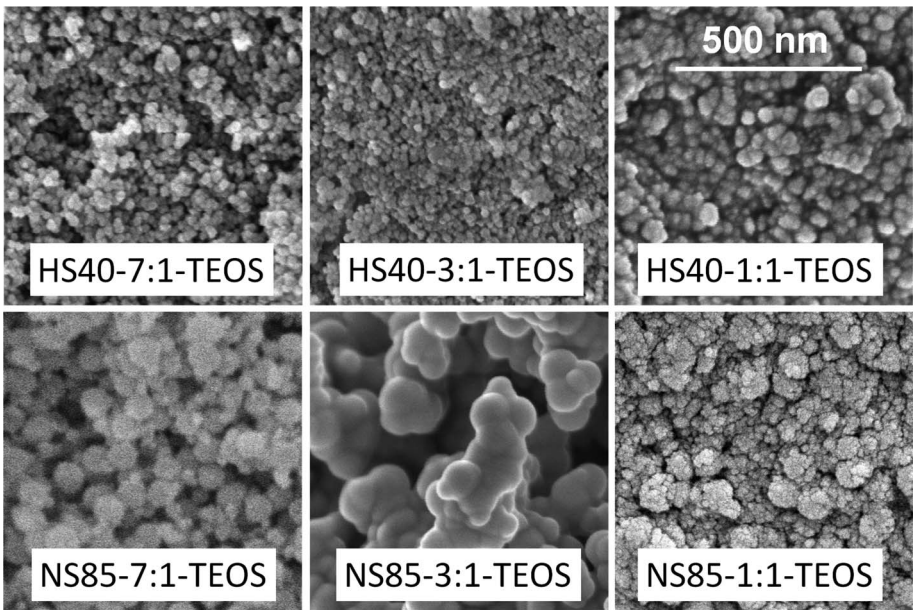

Fig. 4 Particle-scale SEM micrographs of TEOS cross-linked gels with different SNP sizes (HS40 ~12 nm and NS85 ~50 nm) and SNP to crosslinker ratios (the scale-bar is the same for all images).

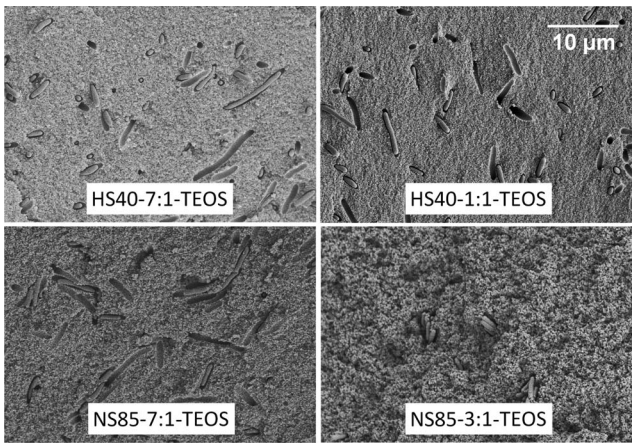

Fig. 5 Cell-scale SEM micrographs of TEOS cross-linked gels with different SNP sizes (HS40 ~12 nm and NS85 ~50 nm) and SNP to crosslinker ratios (scale-bar is the same for all images).

decreasing trend in load at compressive yield of 7 : 1 gels with increasing particle size. As seen in Fig. 4, for 7 : 1 gels, number of SNPs per volume increases when SNP size is decreased. Therefore, the number of crosslinking sites increased per volume which can explain the increase in compressive strength. MTES cross-linked gels had higher compressive strength than TEOS in TM40-7 : 1 and NS125-7 : 1 formulations. However, a wider range of gel formulations need to be tested to evaluate the effect of crosslinker functionality on mechanical strength of the gels. We selected hemispherical beads for mechanical testing since they were utilized in the flow-through biocatalytic activity assays. However we suspect that the geometry of the samples has contributed to variation in the results, due to non-perfect curvature of the samples.

In summary, it was observed that during gelation, silicon alkoxide crosslinkers can react with surface silanol groups of SNPs and deposit on the particles and/or form aggregates by condensation reactions. Note that even though the silicon alkoxide crosslinkers are stable after hydrolysis in low pH conditions, introduction of the SNPs in neutral pH catalyzes the condensation reactions. Therefore, it is unavoidable to obtain small aggregates of silica formed by silicon alkoxides. Higher SNP to crosslinker ratios favor microstructures dictated by SNP size as shown in Fig. 4, which also increases the diffusivity of the gel. However, the gels with higher diffusivity values (such as NS125-7 : 1-TEOS, NS125-7 : 1-MTES and NS125-3 : 1-MTES) have lower mechanical strength under compressive loading as can be seen in Fig. 6.

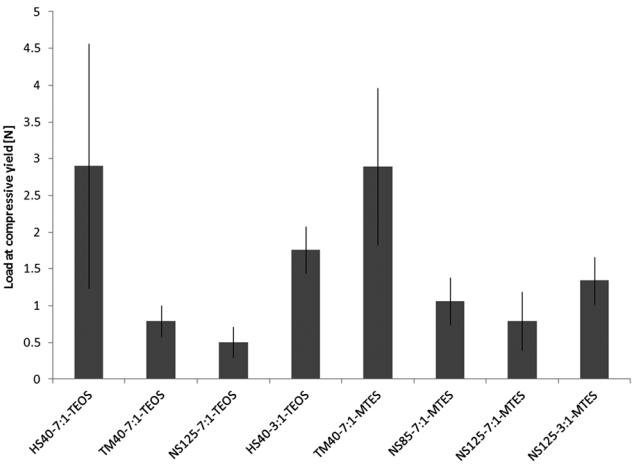

Fig. 6 Mechanical properties of the selected silica gels.

Bacterial biocatalyst: cell viability and catalytic activity

Cell viability assay results are shown in Fig. 7 (Gel formulations with no viable cells on day 0 are not shown). On day 0, TEOS cross-linked samples with 7 : 1 and 3 : 1 SNP to crosslinker ratio had viable cells with comparable CFU counts, whereas 1 : 1 SNP to crosslinker ratio samples had no viable cells. MTES cross-linked samples had viable cells with 7 : 1 SNP to crosslinker ratio, but not with 3 : 1 SNP to crosslinker ratio. On day 4, only one of the TEOS cross-linked samples (HS40-7 : 1-TEOS) had viable cells. MTES-7 : 1 gels, however, had viable cells even though the CFU count has decreased 1–2 orders of magnitude on average. It is well known that ethanol is detrimental to the bacteria and time-scale of alcohol's detrimental effects is very rapid. Therefore, we expect that all the viability loss in day 0 is due to alcohol. However, alcohol does not explain the decrease in viability after 4 day storage period. One possible explanation is the aging of the material and stiffening of the gel inducing increased mechanical stress on the cells. Another possible explanation is the desiccation of the bacteria due to lack of water. For either theory, we were unable to find evidence based on micrographs obtained after 4 days of storage (data not shown).

Transient biocatalytic activity results show hydroxyatrazine (degradation product of atrazine by the encapsulated AtzA biocatalyst) concentration in the initially 150 μM (~32.4 ppm) aqueous atrazine buffer solution after an hour of incubation with the catalytic biomaterial. Results for TEOS and MTES cross-linked gels are shown in Fig. 8(a) and (b). For TEOS cross-linked gels, the most prominent factor affecting biocatalytic activity was SNP to crosslinker ratio. On day 0, 7 : 1 and 3 : 1 samples had comparable biocatalytic activity for all SNP sizes; whereas 1 : 1 samples had significantly lower activity. On day 4, 7 : 1 samples retained 50 to 90% of their activity (except NS85) while 3 : 1 samples lost more than 50% activity. We did not observe a trend based on the SNP size. Based on these observations, we did not proceed with the 1 : 1 ratio for the MTES cross-linked gels. For MTES cross-linked gels, 7 : 1 and 3 : 1 samples had comparable biocatalytic activity for all SNP sizes on day 0, similar to the TEOS case. Likewise on day 4, 7 : 1 samples retained 60 to 90% of their activity (except HS40) while most of the 3 : 1 samples lost more than 90% of activity (except NS125). Unlike the previous case, we could observe an apparent trend based on the SNP size where activity increased slightly with increasing SNP size. MTES cross-linked gels had higher activity than TEOS gels on day 0 for all SNP sizes and SNP to crosslinker ratios. On day 4, most of the 7 : 1 gels with MTES crosslinker had higher activity (except HS40) and 3 : 1 gels with both TEOS and MTES had comparably low activity, except for NS125-3 : 1-MTES. We selected 8 gels out of 20 to proceed with the mechanical tests, based on their activity on day 4.

It was shown in a previous study that biocatalytic activity does not require cell viability[24] and MTES-3 : 1 results in Fig. 8 confirms this result. Based on the day 0 results in Fig. 7, three conclusions can be drawn:

(1) In most cases, SNP size did not significantly affect viability of the cells.

(2) When SNP to crosslinker ratio was decreased to 1 : 1, cell viability decreased to zero. Note that crosslinker content of the gel increases from 12.5% (7 : 1 ratio) to 25% (3 : 1 ratio) and 50% (1 : 1 ratio) as SNP to crosslinker ratio changes. Since hydrolyzed crosslinker solution also contains produced ethanol during hydrolysis reactions, ethanol content also doubles and quadruples respectively; which would explain the loss of viability.

(3) When the crosslinker with lower functionality was used (MTES), the cell viability diminished in 3 : 1 ratio, even though

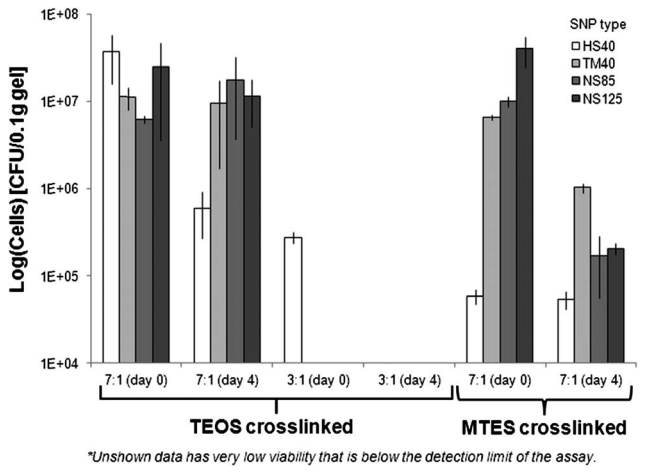

Fig. 7 *E. coli* viability in TEOS and MTES cross-linked biomaterials after encapsulation (day 0 and day 4).

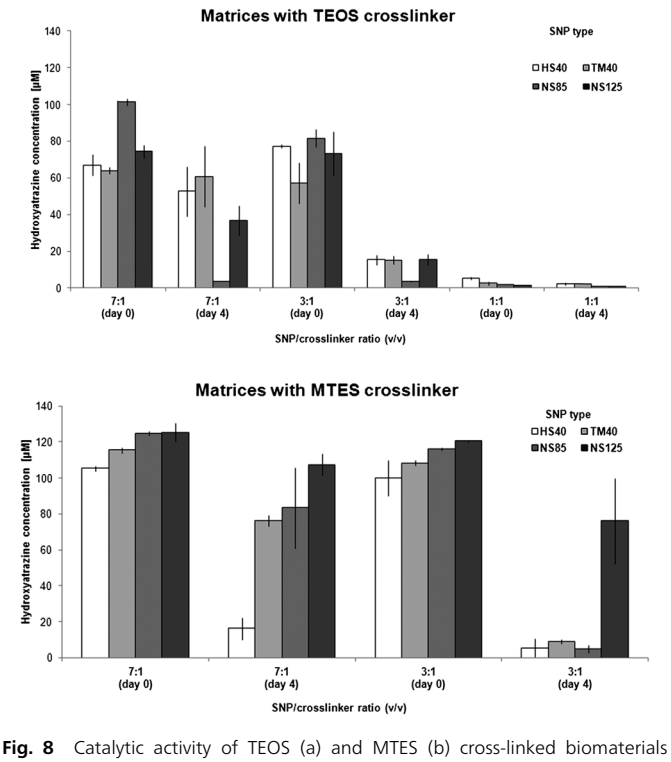

Fig. 8 Catalytic activity of TEOS (a) and MTES (b) cross-linked biomaterials measured by hydroxyatrazine (metabolite) concentration in solution after an hour of incubation with atrazine (day 0 and day 4).

the alcohol content contribution from MTES is lower (assuming full hydrolysis, hydrolyzed MTES solution contains 25% less alcohol than TEOS) due to its lower functionality. Since MTES gels have longer gelation times, bacterial cell membranes are fully exposed to alcohol for longer durations, which can increase the detrimental effect of alcohol. Day 4 results show that all MTES cross-linked gels with 7 : 1 ratio had viability, whereas only HS40-7 : 1 gel had viable cells within TEOS cross-linked gels.

The transient activity results show that biocatalytic activity is affected significantly by SNP to crosslinker ratio and crosslinker functionality, but not SNP size. The loss of activity with decreasing SNP to crosslinker ratio can be explained by chemical composition within the gel. When SNP to crosslinker ratio decreases, water content decreases and alcohol concentration increases and both parameters can hamper enzymatic activity. We have shown that by increasing SNP size, diffusivity of the gel increases. Therefore, we would expect SNP size to have an effect on activity if the overall reaction rate was limited by species transport in the gel. However, no correlation was observed between the catalytic activity rate of the biomaterial and its diffusivity. This result suggests that the reaction rate is either limited by the enzymatic reaction rate of AtzA or a larger transport resistance that occurs at the cell membrane or material/solution interface. It was previously reported that there is about 7% variation in the catalytic activity of free *E. coli* cells expressing AtzA.[24] Consequently, we believe that the variation in the activity of free biocatalyst contributes to the variation of activity results in encapsulated cells. In future studies, reaction kinetics studies should be conducted in both high and low concentrations of atrazine with free *E. coli* cells expressing AtzA to better understand the reaction/diffusion rate limitations on the overall catalytic activity rate. The effects of pH and alcohol content on the catalytic activity rate of the free cells should also be investigated.

Three formulations (HS40-7 : 1-TEOS, TM40-7 : 1-MTES, NS125-7 : 1-MTES) were selected for flow-through biocatalytic activity experiments based on the results of transient activity assays and mechanical testing. We selected HS40-7 : 1-TEOS and TM40-7 : 1-MTES based on their sustained activity during storage (Fig. 3) and superior mechanical strength (Fig. 6), and NS125-7 : 1-MTES based on its superior biocatalytic activity on day 4 (Fig. 3). As a negative control, we used TM40-7 : 1-MTES gel without encapsulated cells. Long-term steady-flow biocatalytic activity assay results (Fig. 9) show that for all the selected gels, the effluent atrazine concentration was sustained below 30% of the influent concentration of 10 ppb for 2 months. It can be observed that effluent concentration of the reactor with the no-cell control gradually reached the influent concentration only after ~7 weeks, suggesting that some portion of atrazine was still being adsorbed by silica gel within that time frame. The difference in effluent concentrations between no cell material and encapsulated cells over the duration of the experiment shows that the removal of atrazine was mostly due to degradation rather than adsorption. Within the reported duration of the experiment, no significant variation in atrazine removal efficiency was observed amongst

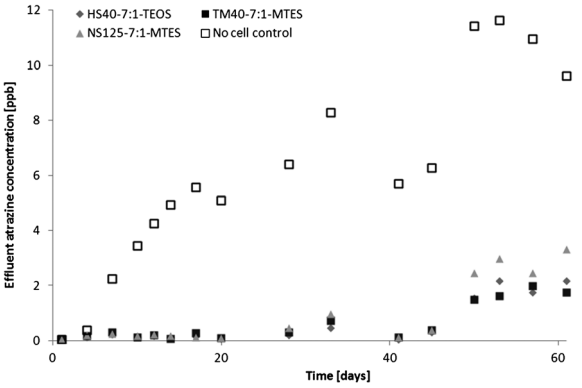

Fig. 9 Long term steady-flow biocatalytic activity of selected biomaterials as demonstrated by measuring effluent concentration of atrazine. The influent concentration was 10 ppb.

different gel formulations. Therefore steady-flow performance of different formulations could not be evaluated. This is primarily due to the long residence time of atrazine solution within the bioreactors, concealing any performance difference between the gels. Higher flow rates need to be investigated in future studies to fully assess the limitations of the developed materials both in terms of their mechanical integrity and degradation activity.

Conclusion

Sol–gel encapsulation of bacterial biocatalysts in silica gel requires a fine balance between obtaining good material properties (mechanical strength, structural integrity, permeability, *etc.*) and preserving biocatalytic activity of the cells. These constraints cause limitations on the design process, oftentimes leading to insufficient material properties or biocatalytic performance. Solving these problems usually involves incorporation of additives, which in turn increases the cost of the material. In this study, we show that by using silicon alkoxide cross-linked silica nanoparticle gels for encapsulation of bacterial biocatalysts, silica gel microstructure can be fine-tuned while preserving good biocatalytic activity. Use of SNPs as the major silica precursor and elimination of the additives significantly reduces the cost of the material, making it a suitable alternative for large scale water treatment applications.

Besides pesticides, other low concentration contaminants in drinking water supplies (pharmaceuticals, personal care products, endocrine disruptors, *etc.*) are also an increasing concern, and studies suggest that water treatment plants cannot completely remove these pollutants by conventional treatment methods.[31] Our results show that the developed catalytic biomaterials can be used to remove trace levels of atrazine in a flow-through packed bed reactor system with high removal efficiency for at least 2 months. Therefore, the developed encapsulation method in this study holds potential to be applied to different bacterial biocatalysts, and can be used for removal of other pollutants from drinking water supplies.

Acknowledgements

This research was supported by a National Science Foundation grant (CBET-0644784) to Alptekin Aksan, a research grant from Syngenta Crop Protection to Lawrence Wackett, Michael Sadowsky and Alptekin Aksan and a BioTechnology Institute grant to Alptekin Aksan and Lawrence Wackett.

References

1 M. A. Snyder, D. Demirgoz, E. Kokkoli and M. Tsapatsis, *Microporous Mesoporous Mater.*, 2009, **118**, 387–395.
2 A. Nieto, S. Areva, T. Wilson, R. Viitala and M. Vallet-Regi, *Acta Biomater.*, 2009, **5**, 3478–3487.
3 J. C. Rooke, A. Leonard and B.-L. Su, *J. Mater. Chem.*, 2008, **18**, 1333–1341.
4 N. Nassif, O. Bouvet, M. N. Rager, C. Roux, T. Coradin and J. Livage, *Nat. Mater.*, 2002, **1**, 42–44.
5 A. C. Patel, S. X. Li, J. M. Yuan and Y. Wei, *Nano Lett.*, 2006, **6**, 1042–1046.
6 A. Leonard, J. C. Rooke, C. F. Meunier, H. Sarmento, J.-P. Descy and B.-L. Su, *Energy Environ. Sci.*, 2010, **3**, 370–377.
7 M. L. Ferrer, L. Yuste, F. Rojo and F. del Monte, *Chem. Mater.*, 2003, **15**, 3614–3618.
8 N. Nassif, C. Roux, T. Coradin, M. N. Rager, O. M. M. Bouvet and J. Livage, *J. Mater. Chem.*, 2003, **13**, 203–208.
9 N. Nassif, A. Coiffier, T. Coradin, C. Roux, J. Livage and O. Bouvet, *J. Sol-Gel Sci. Technol.*, 2003, **26**, 1141–1144.
10 S. Fennouh, S. Guyon, C. Jourdat, J. Livage and C. Roux, *Comptes Rendus De L Academie Des Sciences Serie Ii Fascicule C-Chimie*, 1999, **2**, 625–630.
11 N. Nassif and J. Livage, *Chem. Soc. Rev.*, 2011, **40**, 849–859.
12 C. Y. Oh and J. K. Park, *Bioprocess Eng.*, 1998, **19**, 419–425.
13 A. Coiffier, T. Coradin, C. Roux, O. M. M. Bouvet and J. Livage, *J. Mater. Chem.*, 2001, **11**, 2039–2044.
14 D. Avnir, T. Coradin, O. Lev and J. Livage, *J. Mater. Chem.*, 2006, **16**, 1013–1030.
15 K. S. Finnie, J. R. Bartlett and J. L. Woolfrey, *J. Mater. Chem.*, 2000, **10**, 1099–1101.
16 M. Perullini, M. Amoura, C. Roux, T. Coradin, J. Livage, M. Laura Japas, M. Jobbagy and S. A. Bilmes, *J. Mater. Chem.*, 2011, **21**, 4546–4552.
17 W. H. Organization, Atrazine and I. Metabolites in *Drinking-water*, http://www.who.int/water_sanitation_health/dwq/chemicals/dwq_background_20100701_en.pdf, accessed 6/3, 2013.
18 U. S. E. P. Agency, *Interpreting the Atrazine Drinking Water Monitoring Data*, http://www.epa.gov/oppsrrd1/reregistration/atrazine/atrazine_update.htm, accessed 6/3, 2013.
19 L. Zhu, T. Ma, J. Wang, H. Xie, J. Wang, C. Xin and B. Shao, *Soil Sediment Contam.*, 2011, **20**, 87–97.
20 S. Patricia Galindez-Najera, O. Ramos-Monroy, N. Ruiz-Ordaz, A. Salmeron-Alcocer, C. Juarez-Ramirez, D. Ahuatzi-Chacon, E. Curiel-Quesada and J. Galindez-Mayer, *J. Chem. Technol. Biotechnol.*, 2011, **86**, 554–561.
21 C. Liu, X. Huang and H. Wang, *Desalination*, 2008, **231**, 12–19.
22 S. Klein, R. Avrahami, E. Zussman, M. Beliavski, S. Tarre and M. Green, *J. Ind. Microbiol. Biotechnol.*, 2012, **39**, 1605–1613.
23 G. Buttiglieri, L. Migliorisi and F. Malpei, *Water Sci. Technol.*, 2011, **63**, 1334–1340.
24 E. Reategui, E. Reynolds, L. Kasinkas, A. Aggarwal, M. J. Sadowsky, A. Aksan and L. P. Wackett, *Appl. Microbiol. Biotechnol.*, 2012, **96**, 231–240.
25 M. L. de Souza, M. J. Sadowsky and L. P. Wackett, *J. Bacteriol.*, 1996, **178**, 4894–4900.
26 C. J. Brinker, *J. Non-Cryst. Solids*, 1988, **100**, 31–50.
27 A. M. Siouffi, *J. Chromatogr., A*, 2003, **1000**, 801–818.
28 R. B. Bird, W. E. Stewart and E. N. Lightfoot, *Transport Phenomena*, Wiley, 2007.
29 C. J. Brinker and G. W. Scherer, *Sol-gel science: the physics and chemistry of sol-gel processing*, Academic Press, 1990.
30 P. Innocenzi, M. O. Abdirashid and M. Guglielmi, *J. Sol-Gel Sci. Technol.*, 1994, **3**, 47–55.
31 S. A. Snyder, P. Westerhoff, Y. Yoon and D. L. Sedlak, *Environ. Eng. Sci.*, 2003, **20**, 449–469.

